Published in final edited form as:
Dev Cell. 2012 February 14; 22(2): 418–429. doi:10.1016/j.devcel.2012.01.008.

miR-221 is required for endothelial tip cell behaviors during vascular development

Stefania Nicoli[1], **Carl-Philipp Knyphausen**[1,2], **Lihua J. Zhu**[1,3], **Abirami Lakshmanan**[1], and **Nathan Lawson**[1,*]

[1]Program in Gene Function and Expression, UMass Medical School Worcester, MA 01605 USA

[2]Westfälische Wilhelms-Universität Münster, Schlossplatz 2, D-48149 Münster

[3]Program in Bioinformatics and Integrative Biology

SUMMARY

Angiogenesis requires coordination of distinct cell behaviors between tip and stalk cells. While this process is governed by regulatory interactions between the Vascular endothelial growth factor (Vegf) and Notch signaling pathways, little is known about the potential role of microRNAs. Through deep sequencing and functional screening in zebrafish, we find that *miR-221* is essential for angiogenesis. *miR-221* knockdown phenocopied defects associated with loss of the tip cell-expressed Flt4 receptor. Furthermore, *miR-221* was required for tip cell proliferation and migration, as well as tip cell potential in mosaic blood vessels. *miR-221* knockdown also prevented "hyper-angiogenesis" defects associated with Notch deficiency and *miR-221* expression was inhibited by Notch signaling. Finally, *miR-221* promoted tip cell behavior through repression of two targets: *cyclin dependent kinase inhibitor 1b* (*cdkn1b*) and *phosphoinositide-3-kinase regulatory subunit 1* (*pik3r1*). These results identify *miR-221* as an important regulatory node through which tip cell migration and proliferation are controlled during angiogenesis.

Keywords

microRNA; miR-221; angiogenesis; tip cell; zebrafish

INTRODUCTION

During embryogenesis, vascular development proceeds through two distinct stages (Poole and Coffin, 1989). *De novo* formation of blood vessels, or vasculogenesis, begins with the emergence of angioblast progenitor cells from the lateral mesoderm and migration to target tissues where they coalesce, assemble into cords, and lumenize to form the major blood vessels. Subsequently, smaller caliber vessels sprout from pre-existing ones by angiogenesis(Poole and Coffin, 1989), which requires careful orchestration of distinct cell behaviors between adjacent endothelial cells (Gerhardt et al., 2003). Initial sprouting is driven by pro-angiogenic factors in the surrounding extracellular environment that induce

*Corresponding author: Nathan D. Lawson, Ph.D., Associate Professor, Program in Gene Function and Expression, University of Massachusetts Medical School, 364 Plantation Street, LRB617, Worcester, MA 01605, website: lawsonlab.umassmed.edu, nathan.lawson@umassmed.edu, phone: 508-856-1177.

selected cells to emerge from an established blood vessel. These leading tip cells exhibit extensive filopodia and pathfinding behavior, while trailing stalk cells do not (Gerhardt et al., 2003). In some vascular beds (e.g. mouse retinal vasculature), the vascular plexus grows via proliferation of stalk cells as tip cells migrate, while in others (e.g. zebrafish segmental vessels), tip cells exhibit both migration and proliferation (Gerhardt et al., 2003; Siekmann and Lawson, 2007). Despite these differences, the distinction between tip and stalk cells is an essential conserved process that allows blood vessels to grow while maintaining their connection to the patent vascular system (Thurston et al., 2007).

The signals that coordinate tip and stalk cell behaviors have been the subject of intense investigation. Initial tip cell emergence is driven by Vascular endothelial growth factor A (Vegfa), which is acutely required for tip cell filopodia activity and migration (Gerhardt et al., 2003). Accordingly, tip cells express receptors for both Vegfa (Vegfr-2) and Vegfc (Vegfr-3/Flt4), the latter of which is highly dynamic and becomes restricted to the tip cell during sprouting(Covassin et al., 2006b; Gerhardt et al., 2003; Siekmann and Lawson, 2007; Tammela et al., 2008). Vegfa induces tip cell expression of the Notch ligand, *dll4*, and subsequent Notch activation in the stalk cell suppresses tip cell behaviors, in part, by repressing *flt4* expression (Hellstrom et al., 2007; Lobov et al., 2007 Siekmann, 2007 #901; Tammela et al., 2008). Consistent with this model, mouse or zebrafish embryos lacking *dll4* display excessive blood vessel branching and endothelial proliferation (Hellstrom et al., 2007; Leslie et al., 2007; Siekmann and Lawson, 2007; Suchting et al., 2007), which can be normalized by reducing Vegfr-3/flt4 signaling (Hogan et al., 2009; Siekmann and Lawson, 2007; Tammela et al., 2008). More recent observations have demonstrated competition between endothelial cells for the leading tip cell position during sprouting (Jakobsson et al., 2010). Endothelial cells with lower Vegfr-2 or increased Notch signaling are often excluded from the tip cell position (Jakobsson et al., 2010), consistent with similar results in mosaic zebrafish blood vessels (Siekmann and Lawson, 2007). Thus, tip and stalk cell behaviors are coordinated through negative interactions between the Vegf and Notch pathways. However, little is known about the possible role of post-transcriptional control of this dynamic process.

MicroRNAs are expressed as autonomous transcripts, or are found in introns where they are expressed within pre-mRNA (Ghildiyal and Zamore, 2009). Autonomous microRNA precursors are cleaved in the nucleus by Drosha (Lee et al., 2003), leaving short hairpin RNAs that are transported to the cytoplasm and cleaved by the ribonuclease Dicer (Bernstein et al., 2001; Hutvagner et al., 2001). The mature strand from the resulting double stranded ~22 nucleotide microRNA is subsequently incorporated into a ribonucleoprotein silencing complex (RISC; Czech and Hannon, 2011; Gregory et al., 2005) and used as a complementary guide sequence that binds to sites in the 3′ UTR of a target mRNA. Upon RISC binding, a target transcript is deadenylated leading to its degradation and translational repression (Giraldez et al., 2006; Guo et al., 2010; Wu et al., 2006). Thus, in most cases, microRNAs provide a mechanism for post-transcriptional repression of gene expression. Since microRNAs have been implicated in multiple aspects of vascular growth control (Suarez and Sessa, 2009), we reasoned that they might play a role to coordinate tip and stalk cell behaviors. By applying deep sequencing and functional screening of microRNAs in zebrafish embryos, we identified *mir-221* as an essential regulator of tip cell proliferation and migration.

RESULTS

miR-221 is expressed in embryonic endothelial cells and is required for angiogenesis

To identify candidate microRNAs required for angiogenesis, we sequenced small RNAs from zebrafish endothelial cells at 24 hours post fertilization (hpf), at which time there is extensive vascular growth (Isogai et al., 2003; Siekmann and Lawson, 2007; Figure S1A).

Approximately 20 microRNAs displayed 2 fold or greater enrichment in GFP+ cells isolated from *Tg(kdrl:egfp)*^{la116} embryos compared to GFP- cells and more than 50 were highly expressed (>1000 sequence tags) in GFP+ cells, many of which are also expressed in human endothelial cells (Table S1; Kuehbacher et al., 2007). We also noted hematopoietic-expressed microRNAs (e.g. *miR-223*, *miR-451*) consistent with *kdrl:egfp* expression in hematopoietic cells (Bertrand et al., 2010).

We validated candidate microRNA expression by whole mount *in situ* hybridization using locked nucleic acid (LNA) probes. Candidates were selected based on enrichment (e.g. *miR-20b*) or high expression (e.g. *miR-221*) in *kdrl:gfp*-positive cells. Several candidate microRNAs displayed expression similar to the endothelial-expressed transcription factor, *fli1a*, at 48 hpf including *miR-107*, *miR-20b*, *miR-221*, and *miR-222* (Figure 1A, Table S1, and data not shown). To assess the function of these microRNAs, we injected Morpholinos (MOs) to block their maturation (Figure S1B and data not shown) and observed vascular and overall morphology in *Tg(kdrl:egfp)*^{la116} embryos. In most cases, we noted normal development and ISV formation at 30 hpf, except for *miR-221*-knockdown, which caused partial ISV formation (Figure 1B). We also observed distinct cardiovascular defects associated with loss of other microRNAs. For example, *miR-107*-deficient embryos displayed vascular stability defects (Figure S1C), while embryos lacking *miR-20b* exhibited an apparent block in erythroid differentiation (Figure S1D). Based on our interest in identifying microRNAs involved in angiogenesis, we investigated the function of *miR-221* in greater detail.

Consistent with our deep sequencing data, *miR-221* is detected at high levels in endothelial cells from *Tg(kdrl:egfp)*^{la116} embryos at 24 hpf (Figure S1E). While a high proportion of *miR-221*-deficient embryos displayed partial ISV formation at 30 hpf (Figure 1B, S1F), general embryonic development was not delayed and overall morphology appeared normal (Figure 1B). Loss of *miR-221* did not perturb development or differentiation of structures adjacent to ISVs, such as somites, neural tube, and notochord (Figure S1G). Closer inspection revealed defects in formation of the primordial hindbrain channel, a transient vein in the zebrafish hindbrain (Isogai et al., 2003), in embryos lacking *miR-221*, while the adjacent lateral dorsal aortae formed normally (Figure 1C). We also noted lack of the thoracic duct, a primary lymphatic vessel, at 5 days post fertilization while overall morphology was normal at this stage (Figure 1D, E). A second MO targeting *miR-221* caused the same vascular defects (Figure S1H, I and data not shown). Although there is a high degree of homology between *miR-221* and *miR-222*, both MOs were specific for *miR-221* (Figure S1J) and simultaneous knockdown of *miR-221* and *miR-222* did not enhance or cause additional vascular defects (data not shown). We did not note any changes in expression of either *vegfa*, or its receptor *kdrl* (Figure S2A), which are essential for ISV sprouting, (Covassin et al., 2006b) in *miR-221* deficient embryos. Likewise, ISV and vein-specific expression of *flt4* and artery-specific expression of its ligand *vegfc*, as well as *ephrinb2a*, *notch3*, and *dll4* were not affected by loss of *miR-221* (Figure S2A, B). Circulation and heart function were also normal in *miR-221* deficient embryos (data not shown). Together, these results demonstrate that *miR-221* is highly expressed in endothelial cells and is required for angiogenesis.

miR-221 is required for signaling through the Vegfc/Flt4 pathway

In the zebrafish embryo, *kdrl* and *flt4* cooperate to drive ISV growth, while *flt4* alone is required for vein and lymphatic development and *kdrl* alone is required for artery differentiation and morphogenesis (Covassin et al., 2006b; Habeck et al., 2002; Hogan et al., 2009). Strikingly, the phenotypes associated with loss of *miR-221* were identical to those in embryos lacking *flt4* (Covassin et al., 2006b; Hogan et al., 2009). By contrast, *miR-221*-deficient embryos did not display hallmarks of Vegfa deficiency, such as arteriovenous

circulatory shunts or loss of artery differentiation (data not shown and Figure S2A). These observations suggested that *miR-221* preferentially affects the Vegfc/Flt4 pathway. To determine if this was the case, we first assessed the genetic interaction between *miR-221* and *kdrl* or *flt4* by quantifying ISV length in embryos lacking combinations of these genes. Embryos injected separately with either 1 ng of *flt4* or 5 ng of *miR-221* MO displayed ISVs of normal length at 30 hpf similar to embryos injected with control MO (Figure 2A–C, G). However, co-injection of these sub-phenotypic MO doses resulted in significantly shorter ISVs (Figure 2D, G), similar to a more complete knockdown of either gene alone at higher doses (Figure 2G). Furthermore, we did not observe any enhancement of the ISV defect in embryos co-injected with these higher MO doses (Figure 2G), suggesting that *flt4* and *miR-221* act in the same pathway. By contrast, reduction of *miR-221* in mutant embryos bearing a null $kdrl^{um19}$ allele decreased ISV length compared to control $kdrl^{um19}$ mutant embryos (Figure 2E–G), which normally display variable partial shortening in ISV length (Covassin et al., 2009). The enhanced ISV defect in embryos lacking *miR-221* and *kdrl* is similar to the effect of simultaneously reducing *flt4* and *kdrl* (Covassin et al., 2006b). These observations suggest that *miR-221* acts parallel to *vegfa* and *kdrl* and is likely acting in a common pathway with *vegfc* and *flt4.* Despite this genetic interaction, we did not detect changes in *miR-221* levels in the absence of *flt4* (Figure S2D) and, as noted above, *flt4* levels were normal in *miR-221* deficient embryos (Figure S2A, B).

We next determined if *miR-221* function was required for Vegfc/Flt4 signaling by assessing the response of *miR-221*-deficient embryos to ectopically expressed Vegfc. We used the heat shock 70 (*hsp70*) promoter to inducibly express Vegfc in frame with monomeric red fluorescent protein (mCherry) separated by the viral 2A peptide sequence in zebrafish embryos. Mosaic Vegfc over-expression following heat shock at 15 somite state caused ectopic branching of ISVs along the horizontal myoseptum in control embryos at 33 hpf (Figure 2H, L), but not in *flt4*-deficient embryos (Figure 2I, L) indicating that this effect is dependent on the Flt4 receptor. Likewise, *miR-221* deficient embryos displayed significantly fewer ectopic vessels in response to Vegfc (Figure 2J, L). The loss of ectopic sprouting was not generally attributable to partial ISV formation caused by *flt4*- or *miR-221*-deficiency, as $kdrl^{um19}$ mutant embryos, which also exhibit partial ISV sprouts (see above), form ectopic vessels in response to Vegfc (Figure 2K, L). Together these results suggest that *miR-221* is required for Vegfc/Flt4 signaling during ISV sprouting.

miR-221 is required for endothelial tip cell proliferation and migration

In sprouting blood vessels, *flt4* expression is highly dynamic and becomes restricted to endothelial tip cells (Covassin et al., 2006b; Siekmann and Lawson, 2007; Tammela et al., 2008). Since *miR-221* was required for ISV growth and Vegfc/Flt4-induced angiogenesis, we reasoned that it might play a role in governing endothelial tip cell behaviors. To determine if this was the case, we performed two-photon time-lapse microscopy on embryos lacking or over-expressing *miR-221*. In control embryos, ISVs generally formed by migration of endothelial tip cells from the dorsal aorta followed by a second trailing cell (Figure 3A, 19:30 and 20:54; Supplementary Movie 1), as shown previously (Siekmann and Lawson, 2007). Once reaching the horizontal myoseptum, tip cells in most ISVs divided (Figure 3A, 20:54 to 24:36) and a single daughter cell subsequently migrated dorsally to form the DLAV (Figure 3A, 27:01). In the absence of *miR-221*, the initial rate of movement for tip and trailing cells from the dorsal aorta into the ISV was relatively normal (Figure 3B, 19:30 to 20:50; Supplementary Movie 2; Figure S3A). However, subsequent migration of tip cells from the horizontal myoseptum to the DLAV was significantly slower than in control embryos (for example, compare Figure 3B, 26:51 to Figure 3A, 24:36; Supplementary Movie 2, Figure S3A). In addition, tip cells often failed to divide in *miR-221* deficient embryos (Figure 3B, Supplementary Movie 2). Together, these defects resulted in delayed

formation of the ISV and DLAV, which were ultimately comprised of fewer endothelial cells in *miR-221* deficient embryos (see below). By contrast, injection of *miR-221* duplex induced precocious division of tip cells prior to reaching the horizontal myoseptum (Figure 3C, 19:30 to 20:20; Supplementary Movie 3). In addition, excessive numbers of cells from the dorsal aorta continued to migrate into the ISV (Figure 3C, 20:20 to 23:07), further increasing cell numbers in the ISVs (Figure 3C, 28:37 and see below), although ISV growth rate was not faster than in control embryos (data not shown). Consistent with our time-lapse observations, fewer tip cells in *miR-221*-deficient ISVs incorporated BrdU than in control embryos when pulsed beginning at 20 hpf, while exogenous *miR-221* expression increased BrdU incorporation in cells that contributed to the DLAV (Figure S3B, C). Interestingly, the number of BrdU-positive cells in the dorsal aorta and posterior cardinal vein did not change significantly in either case (Figure S3D), suggesting a preferential effect of *miR-221* on ISV tip cell proliferation. These observations indicate that *miR-221* is required for both migration and proliferation of endothelial tip cells during ISV angiogenesis.

We have previously assessed the potential of an endothelial cell to be a tip cell (referred to hereafter as “tip cell potential”) by determining its ability to contribute to the DLAV, which, based on time lapse analysis, is initially formed from a daughter of the initial ISV tip cell. Using this assay, we have successfully demonstrated that endothelial cells lacking Notch activity, which exhibit excessive proliferation and migration, preferentially localize to the DLAV (Siekmann and Lawson, 2007), while recent studies demonstrate a similar behavior for endothelial cells partially deficient in plexin signaling (Zygmunt et al., 2011). To assess the tip cell potential of *miR-221*-deficient or over-expressing cells, and to confirm the endothelial autonomy of these effects, we transplanted donor cells from *Tg(fli1a:egfp)*^{y1} embryos injected with *miR-221* MO or *miR-221* duplex, respectively, into wild type *Tg(kdrl:ras-cherry)*^{s916} host embryos. Control donor cells contributed well to all host blood vessels in the zebrafish trunk (Figure 4A, D, E; control MO into wt, N=20; control duplex into wt, N=16), while *miR-221*-deficient endothelial cells contributed less frequently to the DLAV (Figure 4B, D; N=17), consistent with their reduced proliferation and migratory rates observed in time-lapse analysis (see above). On the contrary, donor cells expressing exogenous *miR-221* showed an enhanced ability to contribute to the DLAV (Figure 4C, E; N=21). Donor cells with either gain or loss of *miR-221* expression otherwise contributed to most other blood vessel positions, ruling out a general defect in endothelial cell specification (Figure 4A–E). Furthermore, ISV formation was normal in embryos where *miR-221*-deficient donor cells contributed only to surrounding neural tube or somite tissue but not endothelial cells (Figure 4F; N=10). Thus, *miR-221* increases tip cell potential during ISV angiogenesis and does so in an endothelial autonomous manner.

miR-221 is negatively regulated by Notch signaling

The defects caused by exogenous *miR-221* were similar to those associated with loss of *dll4* (Hellstrom et al., 2007; Leslie et al., 2007; Siekmann and Lawson, 2007), suggesting an antagonistic relationship between *miR-221* and Notch signaling. Therefore, we investigated the genetic interaction between *miR-221* and *dll4* by comparing ISV length and cell numbers in embryos following knockdown of one or both of these genes. Similar to previous observations, *dll4* deficiency resulted in significantly more ISV endothelial cells at 27 hpf than in control embryos (Fig. 5A–B, J), similar to injection of *miR-221* duplex (Fig. 5C, J). By contrast, *mir-221* knockdown significantly decreased cell numbers, as well as ISV length (Fig. 5D, J, K), consistent with time-lapse analysis (see Figure 3). Likewise, simultaneous reduction of *mir-221* and *dll4* decreased ISV cell number and length compared to *dll4* knockdown alone (Figure 5E, J, K). At 35 hpf, *dll4*-deficient embryos displayed excessive cell numbers compared to control embryos (Figure 5F, G, J), while ISVs in *mir-221*-deficient embryos, which have recovered to form a DLAV and exhibit normal ISV length

(Figure 5K, H), displayed fewer ISV cells (Figure 5H, J). Furthermore, *dll4*-deficient embryos lacking *miR-221* displayed normalized numbers of cells similar to wild type ISVs (Figure 5I, J). Taken with our finding that exogenous *miR-221* drives excessive migration and proliferation, these observations suggest that *miR-221* is required for excessive angiogenesis associated with loss of Notch.

Notch signaling blocks angiogenesis, in part, by repressing *flt4* expression (Siekmann and Lawson, 2007). Since *miR-221* acted in the *flt4* signaling pathway, we determined whether it might also be repressed by Notch. In embryos injected with a MO targeting the Rbpsuh DNA binding protein, which is required for Notch signaling (Bailey and Posakony, 1995; Fortini and Artavanis-Tsakonas, 1994), we found that *miR-221* is upregulated (Figure 5L). By contrast, injection of mRNA encoding an activated form of Notch repressed *miR-221* levels when compared to control injected embryos (Figure 5L). To demonstrate that the effect of Notch signaling on *miR-221* levels was occurring in endothelial cells, we utilized an endothelial autonomous microRNA sensor assay (Nicoli et al., 2010). In this case, we generated a transgenic line (*Tg(fli1ep:egfp;mcherry-pik3r1)*^{um28}) using an endothelial cell-specific bicistronic vector driving *mcherry* fused to a 3′ UTR containing two *miR-221* binding sites (Figure S4A and see below) and *egfp* fused to a control 3′UTR. *Tg(fli1ep:egfp;mcherry-pik3r1-utr)*^{um28} embryos exhibited robust green fluorescence in trunk blood vessels at 28 hpf, while *mcherry* levels appeared lower (Figure 5M). Consistent with *miR-221*-mediated repression of the *mcherry* transcript, we observed increased red fluorescence in *Tg(fli1ep:egfp;mcherry-pik3r1)*^{um28} embryos injected with *miR-221* MO (Figure 5M, S4B). By contrast, Mcherry expression was significantly repressed following injection of *rbpsuh* MO (Figure 5M, S4B), consistent with our observation that *miR-221* levels are increased in Notch deficient embryos (Figure 5L). Similar results were observed with a second 3′ UTR bearing *miR-221* sites (see below and Figure S4B, C). Taken together, our results demonstrate that Notch negatively regulates *miR-221* to block endothelial tip cell proliferation and migration.

Repression of two distinct targets by *miR-221* is required for angiogenesis

In tumor cells *miR-221* drives proliferation by repressing *cyclin dependent kinase inhibitor 1b* (*cdkn1b*; Galardi et al., 2007), which blocks cell cycle progression. Since our studies demonstrated a block in endothelial proliferation in *miR-221* deficient embryos, *cdkn1b* was a viable candidate target during angiogenesis. In addition, we identified *pik3r1*, the p85-alpha regulatory subunit of the phosphoinositide-3-kinase (PI3K) complex, as a candidate target of *miR-221*. Given the importance of PI3K signaling in vascular development (Graupera et al., 2008), we reasoned that this transcript was also a possible functional target of *miR-221* during ISV angiogenesis.

Both *cdkn1b* and *pik3r1* 3′ UTRs contain *miR-221* binding sites (Figure S4A and data not shown) and were repressed by *miR-221* in whole embryo reporter assays (Figure 6A–D) and endothelial cells *in vivo* (Figure 5M, S4B, C). We also detected low-level expression of both transcripts in the trunk blood vessels and isolated *kdrl:egfp* cells (Figure S5A, B). Consistent with the possibility that increased levels of *cdkn1b* and *pik3r1* contributed to defects associated with loss of *miR-221* (see above), overexpression of *cdkn1b* or *pik3r1*, or both together, reduced ISV length and cell numbers (Figure 6E, F), without an overt affect on general development (Figure S5C). Furthermore, mosaic analysis demonstrated that cells expressing both *pik3r1* and *cdkn1b* contribute less frequently to the tip cell position than control (Figure 6G; control mRNA>wt, N=20, *cdkn1b*/*pik3r1* mRNA>wt, N=25), similar to *miR-221* deficient cells (Figure 4B, D). These results indicate that increased levels of *cdkn1b* and *pik3r1* can negatively affect tip cell potential in an endothelial autonomous manner, further supporting that they are normally targeted by *miR-221* during ISV sprouting.

Our results suggest that *miR-221* controls ISV growth by inducing proliferation and PI3K activity through repression of *cdkn1b* and *pik3r1*, respectively. To further investigate the importance of proliferation and PI3K during ISV growth, we treated embryos at 20 hpf with either 5-hydroxyurea and aphidocolin (HUA/AP) to block cell cycle or LY294002 to inhibit PI3K. In both cases, we observed a significant decrease in ISV length and cell number (Fig. 7A–C), although embryos were normal and did not exhibit changes in *vegfa or kdrl* expression (Figure S5D and data not shown). The decrease in ISV cell number was more modest in LY294002-treated embryos than those treated with HUA/AP (Figure 7C). Furthermore, similar to *miR-221* knockdown, HUA/AP, prevented BrdU incorporation into ISV tip cells while LY294002 did not (Figure 7A, D), suggesting that PI3K inhibition does not affect endothelial cell proliferation during sprouting. Our results demonstrate that *pik3r1* over-expression and PI3K inhibition similarly blocked ISV growth, suggesting that increased *pik3r1* in the absence of *miR-221* blunts PI3K signaling output. To determine if this was the case, we generated transgenic zebrafish (referred to as *Tg(fli1ep:phaktegfp-2A-mcherry)*^{um63}) bearing EGFP fused to the pleckstrin homology domain of human Akt1 (PH-AKT-EGFP), which localizes to the membrane in response to PI3K activation (Astoul et al., 1999), and a co-expressed red fluorescent protein. In *Tg(fli1ep:phaktegfp-2A-mcherry)*^{um63} embryos lacking *miR-221*, we observed decreased filopodial localization of PH-AKT-EFP compared to control (Figure S5E, F). Furthermore, partial reduction of *pik3r1* to levels that do not affect ISV formation (see below) restores filopodial PH-AKT-EGFP localization in *miR-221*-deficient *Tg(fli1ep:phaktegfp-2A-mcherry)*^{um63} embryos (Figure S5E, F). These observations suggest that increased levels of *pik3r1* in the absence of *miR-221* cause reduced or mis-localized PI3K output in sprouting endothelial cells, which contributes to the observed defects in ISV growth.

Our results suggested that upregulation of *pik3r1* and *cdkn1b* is the likely cause of ISV growth defects in *miR-221* deficient embryos. If this were the case, then reducing their levels would rescue the phenotypes in *miR*-221 deficient embryos. To investigate this possibility, we injected embryos with MOs to inhibit splicing of *cdkn1b* or *pik3r1* (Figure S6A–D). In all cases, we co-injected *tp53* MO to eliminate off-target toxicity. Reduction of *tp53* alone did not rescue defects associated with *miR-221* deficiency (Figure 8A, E, J, L). Wild type embryos lacking *cdkn1b* exhibited excessive numbers of ISV endothelial cells (Figure 8A, B, I), similar to embryos injected with *miR-221* duplex (see Figure 5C, J), but were otherwise normal (Figure S6D). Embryos injected with 10 ng of MO to reduce *pik3r1* levels displayed variable shortening of ISV length and a slight, but non-significant decrease in ISV cell numbers and were otherwise overtly normal (Figure 8C,I,K; S6B–D). Injection of 5 ng *pik3r1* MO did not cause a phenotype (Figure 8D, I, K). We attempted to rescue *miR-221* deficiency by co-injecting 5 ng of either *cdkn1b* or *pik3r1* MO with 10 ng of *miR-221* MO. In both cases, we observed a partial restoration of ISV length, although not to control levels (Figure 8E–G, L). Interestingly, knockdown of *cdkn1b*, but not *pik3r1*, restored ISV endothelial cell number to control levels in the absence of *miR-221* (Figure 8J), consistent with the differential effects of HUA/AP and LY294002 on endothelial proliferation and ISV growth noted above. Simultaneous knockdown of *ckdn1b* and *pik3r1* in *miR-221* deficient embryos fully restored both ISV length and cell number (Figure 8H, J, L), indicating that these two targets together mediated the function of *miR-221* during ISV growth. Furthermore, endothelial cells with reduced levels of *cdkn1b* and *pik3r1* localized to the DLAV at a greater frequency than control cells in mosaic embryos (Figure 8M; control MO data are same as those shown in Figure 4; *cdkn1b*/*pik3r1* MO>wt, N=24), similar to cells expressing exogenous levels of *miR-221* (see Figure 4E). Thus, *miR-221* induces tip cell proliferation through down-regulation of *cdkn1b* and promotes optimal PI3K output by reducing *pik3r1*. Together, these effects contribute to endothelial tip cell migration and proliferation during angiogenesis.

DISCUSSION

The ability of an endothelial cell to dynamically respond to pro-angiogenic cues is essential to coordinate distinct cellular behaviors with its neighbors. Without this coordination, productive angiogenesis is hindered. Our present work provides evidence that post-transcriptional regulation by microRNAs plays an important role in this process. In particular, we identify *miR-221* as an essential regulator of angiogenesis in embryonic zebrafish and provide evidence that supports a role for *miR-221* in endothelial tip cell proliferation and migration.

miR-221 appears to act in sprouting endothelial cells through repression of two distinct target transcripts: *pik3r1* and *cdkn1b*. Our results suggest that these target genes control distinct tip cell behaviors. While *miR-221*-mediated down-regulation of *cdkn1b* was required for proliferation, PI3K signaling was dispensable for this behavior in tip cells. Although repression of *pik3r1* by microRNAs in other contexts can cause p53-dependent apoptosis (Park et al., 2009), endothelial tip cell survival appeared normal following loss of *miR-221*, *pik3r1*, or PI3K signaling and *tp53* knockdown did not rescue *miR-221* deficiency. Instead, we believe that *pik3r1* is important for tip cell migration, consistent with the role for the PI3K catalytic p110α subunit in endothelial cells (Graupera et al., 2008). Our results further suggest that *miR-221* appropriately tunes PI3K signaling output by controlling the levels of a PI3K regulatory subunit. Pik3r1 usually exists in a 1:1 ratio with a catalytic subunit of the PI3K signaling complex (Geering et al., 2007), such as p110α, and both proteins are otherwise unstable(Yu et al., 1998). Pik3r1 inhibits the catalytic subunits, but is also required for PI3K activity following membrane localization of the Pik3r1/p110 complex and activation by a receptor tyrosine kinase (Vanhaesebroeck et al., 2010). A central question is how increased Pik3r1 may alter PI3K signaling to block sprouting. In some contexts, Pik3r1 acts independently of PI3K catalytic subunits (Garcia et al., 2006), suggesting that increased Pik3r1 may interfere with other signaling pathways required for angiogenesis. However, in this case excess Pik3r1 would not affect PI3K output, yet we observe decreased PI3K activity in the filopodia of *miR-221* deficient ISVs. A more likely possibility is that increased Pik3r1 alters the appropriate balance in regulatory and catalytic subunits, which can be composed of several different isoforms that are present in endothelial cells (Graupera et al., 2008). In turn, a shift in stoichiometry may squelch receptor tyrosine kinase signaling output and PI3K activity. It is also possible that these changes lead to inappropriate subcellular localization of PI3K complexes. In this regard, it is of note that PI3K signaling is active in endothelial filopodia in developing ISVs. Increased Pik3r1 may alter the subcellular localization of PI3K complexes, thereby reducing filopodia PI3K activity, possibly without a change in total cellular PI3K output. In any event, microRNA regulation of PI3K signaling appears to be an emerging theme in the control of this crucial signaling regulator as *miR-126* similarly regulates Vegfr-2 signaling output through modulation of Pik3r2 (Fish et al., 2008; Wang et al., 2008).

The importance of *miR-221* for endothelial tip cell migration and proliferation is consistent with its requirement for signaling through *flt4*. Interestingly, neither *vegfc*, nor *flt4* expression is regulated by *miR-221*, while *miR-221* expression is normal in *flt4*-deficient embryos. We believe that the central point of interaction between *miR-221* and *flt4* is at the level of *pik3r1* regulation. Pik3r1 possesses SH2 domains to facilitate interaction with activated receptor tyrosine kinases and is known to interact with Flt4 following binding to Vegfc (Wang et al., 2004). Thus, *miR-221* may directly affect Flt4 signaling output through its regulation of *pik3r1* levels. While *miR-221* expression is independent of *flt4* itself, we find that it is repressed by Notch activation, similar to *flt4*. Together, our findings suggest a model in which *miR-221* promotes migration and proliferation by potentiating *flt4* signaling through regulation of *pik3r1*, while repressing *cdkn1b*. By contrast, Notch activation in stalk

cells represses both *flt4* and *miR-221*. Subsequently, *cdkn1b* levels increase to limit proliferation, while an increase in *pik3r1* serves to dampen, or qualitatively shift PI3K output.

In contrast to our findings, exogenous *miR-221* is anti-angiogenic in human venous or lymphatic endothelial cells (Chen et al., 2010; Poliseno et al., 2006; Wu et al., 2011). These effects were mediated through numerous distinct targets depending on the study and included the ETS1 transcription factor (Zhu et al., 2011), the stem cell factor receptor C-KIT (Poliseno et al., 2006), and the transcriptional repressor ZEB2 (Chen et al., 2010). *miR-221* can also increase lymphocyte adhesion through repression of ETS1, leading to a decrease in angiotensin II expression (Zhu et al., 2011). Interestingly, this latter work did not note a migration defect in response to *miR-221* over-expression, as cited in other studies. A possible explanation for these discrepancies is that *miR-221* levels vary significantly in response to both serum and Vegfa (Chen et al., 2010; Suarez et al., 2008), suggesting that growth conditions influence microRNA function in cultured cells. These observations raise the possibility that *miR-221* governs context-specific changes in endothelial behavior depending on cell type or developmental stage. Thus, while *miR-221* is an important pro-angiogenic signal during embryonic development, it may play different roles in the mature circulatory system.

While *miR-221* is only modestly enriched in endothelial cells and is present at high levels in non-endothelial cell types, *miR-221* deficiency caused remarkably specific developmental vascular defects. There may several reasons for this observation. First, MOs only provide partial knockdown and the observed phenotypes may be manifest only in cell types (e.g. endothelial tip cells) where high gene dosage is required. Second, *miR-221*-deficient embryos may display subtle defects in other tissues and developmental processes. Indeed, the observed vascular defects were only obvious when using a transgenic background to visualize blood vessel morphology. Thus, more careful molecular and cellular analysis applied to other organ systems may reveal further defects associated with *miR-221* reduction. Finally, microRNAs play an important regulatory role by tuning gene expression to appropriate levels. As such, single microRNA deficiency often has very subtle effects on animal development. In this regard our findings are consistent with those in other models. Interestingly, we also noted specific cardiovascular defects associated with knockdown of other microRNAs (e.g. *miR-107* and *miR-20b*), suggesting a widespread role for small RNAs in vascular development. Further screening of microRNA function in zebrafish will likely reveal additional roles for small RNAs in vascular formation, function and homeostasis.

EXPERIMENTAL PROCEDURES

Zebrafish lines

Zebrafish used in this study are described in Supplementary Experimental Procedures.

miRNA library preparation, deep sequencing, and analysis

Endothelial cells were isolated from *Tg(kdrl:egfp)*^{la116} embryos as previously(Covassin et al., 2006a). Small RNA (18–24 nt) purification, adapter ligation, cDNA synthesis and library amplification were performed as described (Gu et al., 2009). Deep sequencing was performed at the Center for AIDS Research at UMass Medical School. Reads were mapped to known zebrafish microRNAs using the latest version of mirDeep (Friedlander et al., 2008).

Northern blot analysis, in situ hybridization, and quantitative PCR

For Northern analysis, 5 to 10 μg of total RNA was resolved on a 15% acrylamide/7 M urea gel and transferred by electrophoresis to positively charged nylon membrane (Millipore) using a Trans-Blot SD apparatus (Biorad). Hybridization and detection using digoxigenin (DIG)-labeled locked nucleic acid (LNA) probes (Exiqon) were performed as described (Kloosterman et al., 2006). Whole mount in situ hybridization using LNA or antisense RNA probes was performed as previously (Kloosterman et al., 2006; Nicoli et al., 2010). miRNA-quantitative-PCR was performed using the miScript PCR system (Qiagen). Probe and primer sequences can be found in the Supplementary Experimental Procedures.

Morpholino and mRNA injections

MO sequences and primers designed for RT-PCR validation are described in Supplementary Experimental Procedures. Knockdown of the zebrafish *cdkn1b* and *pik3r1* genes was accomplished using MOs targeting splice junctions within these genes which were validated by RT-PCR and qRT-PCR on RNA isolated from injected embryos. MOs targeting *rbpsuh*, *flt4* and *dll4* are described elsewhere (Covassin et al., 2006b; Siekmann and Lawson, 2007). MOs were synthesized by Gene Tools, LLC and dissolved in DEPC water.

microRNA sensor assays

Whole embryo and endothelial autonomous microRNA sensor assays were carried out as previously(Nicoli et al.). For details see Supplementary Experimental Procedures.

Western blot

10 to 20 embryos injected with 3′utr sensor and control mRNAs at 24 hpf were dechorionated and triturated in calcium free ringer solution (Covassin et al., 2006a) and lysed as described (Rand et al., 2004). 40 μg of total protein was separated on a 12 % SDS-PAGE gel. Western blotting was performed according to standard protocols. GFP and Cherry were sequentially detected using rabbit anti-GFP (1:1000, Invitrogen) and rabbit anti-DsRed (1:1000, Clontech), respectively, followed by chemiluminscent immunodetection using anti-rabbit HRP conjugate (1:20,000, Invitrogen).

Chemical treatments, BrdU incorporation, and immunohistochemistry

To block cell division, we treated embryos simultaneously with 150 μM aphidicolin (Sigma) and 20 mM hydroxyurea (Sigma) as described (Lyons et al., 2005). To block PI3K signaling we used 25 μM LY294002 (Sigma). Drug treatments were performed at 20 hpf on dechorionated embryos in agarose-coated dishes. BrdU labeling was performed by injection of 50 mM BrdU in 0.2 M KCl directly into the yolk of *Tg(kdrl:egfp)*^{la116} embryos. Embryos were injected at 20 hpf, transferred to embryo media, and incubated at 28.5°C until 28 hpf. For whole mount immunostaining, embryos were fixed in 4% paraformaldehyde for 2 hours at room temperature and transferred to methanol overnight at −20°C. Embryos were rehydrated to PBST (PBS + 0.5% Triton X-100) and incubated in 2N HCl for 1 hour at room temperature, washed in PBST and placed in blocking solution (PBST + 1% DMSO + 1% BSA + 0.2% goat serum) for 30 minutes at room temperature. To detect BrdU, embryos were immunostained with Alexa-594 anti-BrdU antibody (1:200, Invitrogen) and Alexa-488 anti-GFP antibody (1:300, Invitrogen).

Image acquisition and vessel measurements

Whole mount live and fixed embryos were analyzed using a MZFLIII microscope equipped with epifluorescence. Digital images were captured using a Zeiss mRC digital camera and AxioVision software. Confocal stacks in green (ex. 488 nm laser) and red (ex. 651 nm laser) channels were acquired sequentially using a Leica SP2 confocal microscope. Two-photon

imaging was performed using a LSM7 MP Laser scanning microscope (Zeiss) equipped with a Chameleon Ti:Sapphire pulsed laser (Coherent, Inc.) and images acquired using ZEN 2009 software. For detection of BrdU and Egfp in *Tg(kdrl:egfp)*^{la116} embryos, we sequentially scanned embryos at 1040 nm (70% power) and 920 nm (20% power). Measurements of ISVs were made straight from the edge of the aorta to the leading edge of the sprout. 2-dimensional projections were generated using Imaris (Bitplane). Except where otherwise indicated, all pairwise comparisons were analyzed for significance using a Student's 2-tailed t-test. Error bars in all graphs represent standard deviation (SD).

Mosaic analysis

Transplantations were performed as described (Covassin et al., 2009). Donors were injected with 10 ng of control MO or *miR-221* MO to assess loss-of-function effects or 500 μM of *miR-221* duplex or control duplex to assess gain-of-function effects. The contribution of donor cells was assigned as a percentage of total number of host embryos that display GFP endothelial cells in the indicated vessels. To assess non-autonomous effects, donor cells were injected with miniRuby (Invitrogen) and transplanted into *Tg(fli1a:egfp)*^{y1} embryos. To determine cell autonomous function of *pik3r1* and *cdkn1b*, donor embryos were co-injected with 5 ng of *cdkn1b* and 5 ng of *pik3r1* MOs or 200 pg of *cdkn1b* and 300 pg of *pik3r1* mRNA respectively. Control transplants were performed using donors injected with 500 pg *mcherry* mRNA. The proportions of embryos exhibiting contribution to each vessel type following the indicated experimental manipulations were compared using Fisher's exact test.

Supplementary Material

Refer to Web version on PubMed Central for supplementary material.

Acknowledgments

We thank Jacques Villefranc and Arndt Siekmann for critical review of the manuscript. We are grateful to Daryl Conte and Craig Mello for providing a protocol for small RNA library construction. We thank Tom Smith for excellent technical assistance and John Polli for fish care. This work was supported by R01HL093467 awarded to N. D. L.

References

Astoul E, Watton S, Cantrell D. The dynamics of protein kinase B regulation during B cell antigen receptor engagement. The Journal of cell biology. 1999; 145:1511–1520. [PubMed: 10385529]

Bailey AM, Posakony JW. Suppressor of hairless directly activates transcription of enhancer of split complex genes in response to Notch receptor activity. Genes Dev. 1995; 9:2609–2622. [PubMed: 7590239]

Bernstein E, Caudy AA, Hammond SM, Hannon GJ. Role for a bidentate ribonuclease in the initiation step of RNA interference. Nature. 2001; 409:363–366. [PubMed: 11201747]

Bertrand JY, Chi NC, Santoso B, Teng S, Stainier DY, Traver D. Haematopoietic stem cells derive directly from aortic endothelium during development. Nature. 2010; 464:108–111. [PubMed: 20154733]

Chen Y, Banda M, Speyer CL, Smith JS, Rabson AB, Gorski DH. Regulation of the expression and activity of the antiangiogenic homeobox gene GAX/MEOX2 by ZEB2 and microRNA-221. Molecular and cellular biology. 2010; 30:3902–3913. [PubMed: 20516212]

Covassin L, Amigo JD, Suzuki K, Teplyuk V, Straubhaar J, Lawson ND. Global analysis of hematopoietic and vascular endothelial gene expression by tissue specific microarray profiling in zebrafish. Dev Biol. 2006a; 299:551–562. [PubMed: 16999953]

Covassin LD, Siekmann AF, Kacergis MC, Laver E, Moore JC, Villefranc JA, Weinstein BM, Lawson ND. A genetic screen for vascular mutants in zebrafish reveals dynamic roles for Vegf/Plcg1 signaling during artery development. Dev Biol. 2009; 329:212–226. [PubMed: 19269286]

Covassin LD, Villefranc JA, Kacergis MC, Weinstein BM, Lawson ND. Distinct genetic interactions between multiple Vegf receptors are required for development of different blood vessel types in zebrafish. Proc Natl Acad Sci U S A. 2006b; 103:6554–6559. [PubMed: 16617120]

Czech B, Hannon GJ. Small RNA sorting: matchmaking for Argonautes. Nature reviews Genetics. 2011; 12:19–31.

Fish JE, Santoro MM, Morton SU, Yu S, Yeh RF, Wythe JD, Ivey KN, Bruneau BG, Stainier DY, Srivastava D. miR-126 regulates angiogenic signaling and vascular integrity. Dev Cell. 2008; 15:272–284. [PubMed: 18694566]

Fortini ME, Artavanis-Tsakonas S. The suppressor of hairless protein participates in notch receptor signaling. Cell. 1994; 79:273–282. [PubMed: 7954795]

Friedlander MR, Chen W, Adamidi C, Maaskola J, Einspanier R, Knespel S, Rajewsky N. Discovering microRNAs from deep sequencing data using miRDeep. Nature biotechnology. 2008; 26:407–415.

Galardi S, Mercatelli N, Giorda E, Massalini S, Frajese GV, Ciafre SA, Farace MG. miR-221 and miR-222 expression affects the proliferation potential of human prostate carcinoma cell lines by targeting p27Kip1. J Biol Chem. 2007; 282:23716–23724. [PubMed: 17569667]

Garcia Z, Silio V, Marques M, Cortes I, Kumar A, Hernandez C, Checa AI, Serrano A, Carrera AC. A PI3K activity-independent function of p85 regulatory subunit in control of mammalian cytokinesis. The EMBO journal. 2006; 25:4740–4751. [PubMed: 17024187]

Geering B, Cutillas PR, Nock G, Gharbi SI, Vanhaesebroeck B. Class IA phosphoinositide 3-kinases are obligate p85-p110 heterodimers. P Natl Acad Sci USA. 2007; 104:7809–7814.

Gerhardt H, Golding M, Fruttiger M, Ruhrberg C, Lundkvist A, Abramsson A, Jeltsch M, Mitchell C, Alitalo K, Shima D, et al. VEGF guides angiogenic sprouting utilizing endothelial tip cell filopodia. J Cell Biol. 2003; 161:1163–1177. [PubMed: 12810700]

Ghildiyal M, Zamore PD. Small silencing RNAs: an expanding universe. Nature reviews Genetics. 2009; 10:94–108.

Giraldez AJ, Mishima Y, Rihel J, Grocock RJ, Van Dongen S, Inoue K, Enright AJ, Schier AF. Zebrafish MiR-430 promotes deadenylation and clearance of maternal mRNAs. Science. 2006; 312:75–79. [PubMed: 16484454]

Graupera M, Guillermet-Guibert J, Foukas LC, Phng LK, Cain RJ, Salpekar A, Pearce W, Meek S, Millan J, Cutillas PR, et al. Angiogenesis selectively requires the p110alpha isoform of PI3K to control endothelial cell migration. Nature. 2008; 453:662–666. [PubMed: 18449193]

Gregory RI, Chendrimada TP, Cooch N, Shiekhattar R. Human RISC couples microRNA biogenesis and posttranscriptional gene silencing. Cell. 2005; 123:631–640. [PubMed: 16271387]

Gu W, Shirayama M, Conte D Jr, Vasale J, Batista PJ, Claycomb JM, Moresco JJ, Youngman EM, Keys J, Stoltz MJ, et al. Distinct argonaute-mediated 22G-RNA pathways direct genome surveillance in the C. elegans germline. Mol Cell. 2009; 36:231–244. [PubMed: 19800275]

Guo H, Ingolia NT, Weissman JS, Bartel DP. Mammalian microRNAs predominantly act to decrease target mRNA levels. Nature. 2010; 466:835–840. [PubMed: 20703300]

Habeck H, Odenthal J, Walderich B, Maischein H, Schulte-Merker S. Analysis of a zebrafish VEGF receptor mutant reveals specific disruption of angiogenesis. Current biology : CB. 2002; 12:1405–1412. [PubMed: 12194822]

Hellstrom M, Phng LK, Hofmann JJ, Wallgard E, Coultas L, Lindblom P, Alva J, Nilsson AK, Karlsson L, Gaiano N, et al. Dll4 signalling through Notch1 regulates formation of tip cells during angiogenesis. Nature. 2007; 445:776–780. [PubMed: 17259973]

Hogan BM, Herpers R, Witte M, Helotera H, Alitalo K, Duckers HJ, Schulte-Merker S. Vegfc/Flt4 signalling is suppressed by Dll4 in developing zebrafish intersegmental arteries. Development. 2009; 136:4001–4009. [PubMed: 19906867]

Hutvagner G, McLachlan J, Pasquinelli AE, Balint E, Tuschl T, Zamore PD. A cellular function for the RNA-interference enzyme Dicer in the maturation of the let-7 small temporal RNA. Science. 2001; 293:834–838. [PubMed: 11452083]

Isogai S, Lawson ND, Torrealday S, Horiguchi M, Weinstein BM. Angiogenic network formation in the developing vertebrate trunk. Development. 2003; 130:5281–5290. [PubMed: 12954720]

Jakobsson L, Franco CA, Bentley K, Collins RT, Ponsioen B, Aspalter IM, Rosewell I, Busse M, Thurston G, Medvinsky A, et al. Endothelial cells dynamically compete for the tip cell position during angiogenic sprouting. Nature cell biology. 2010; 12:943–953.

Kloosterman WP, Wienholds E, de Bruijn E, Kauppinen S, Plasterk RH. In situ detection of miRNAs in animal embryos using LNA-modified oligonucleotide probes. Nature methods. 2006; 3:27–29. [PubMed: 16369549]

Kuehbacher A, Urbich C, Zeiher AM, Dimmeler S. Role of Dicer and Drosha for endothelial microRNA expression and angiogenesis. Circ Res. 2007; 101:59–68. [PubMed: 17540974]

Lee Y, Ahn C, Han J, Choi H, Kim J, Yim J, Lee J, Provost P, Radmark O, Kim S, et al. The nuclear RNase III Drosha initiates microRNA processing. Nature. 2003; 425:415–419. [PubMed: 14508493]

Leslie JD, Ariza-McNaughton L, Bermange AL, McAdow R, Johnson SL, Lewis J. Endothelial signalling by the Notch ligand Delta-like 4 restricts angiogenesis. Development. 2007; 134:839–844. [PubMed: 17251261]

Lobov IB, Renard RA, Papadopoulos N, Gale NW, Thurston G, Yancopoulos GD, Wiegand SJ. Delta-like ligand 4 (Dll4) is induced by VEGF as a negative regulator of angiogenic sprouting. P Natl Acad Sci USA. 2007; 104:3219–3224.

Lyons DA, Pogoda HM, Voas MG, Woods IG, Diamond B, Nix R, Arana N, Jacobs J, Talbot WS. erbb3 and erbb2 are essential for schwann cell migration and myelination in zebrafish. Curr Biol. 2005; 15:513–524. [PubMed: 15797019]

Nicoli S, Standley C, Walker P, Hurlstone A, Fogarty KE, Lawson ND. MicroRNA-mediated integration of haemodynamics and Vegf signalling during angiogenesis. Nature. 2010; 464:1196–1200. [PubMed: 20364122]

Park SY, Lee JH, Ha M, Nam JW, Kim VN. miR-29 miRNAs activate p53 by targeting p85 alpha and CDC42. Nature structural & molecular biology. 2009; 16:23–29.

Poliseno L, Tuccoli A, Mariani L, Evangelista M, Citti L, Woods K, Mercatanti A, Hammond S, Rainaldi G. MicroRNAs modulate the angiogenic properties of HUVECs. Blood. 2006; 108:3068–3071. [PubMed: 16849646]

Poole TJ, Coffin JD. Vasculogenesis and angiogenesis: two distinct morphogenetic mechanisms establish embryonic vascular pattern. J Exp Zool. 1989; 251:224–231. [PubMed: 2671254]

Rand TA, Ginalski K, Grishin NV, Wang X. Biochemical identification of Argonaute 2 as the sole protein required for RNA-induced silencing complex activity. Proc Natl Acad Sci U S A. 2004; 101:14385–14389. [PubMed: 15452342]

Siekmann AF, Lawson ND. Notch signalling limits angiogenic cell behaviour in developing zebrafish arteries. Nature. 2007; 445:781–784. [PubMed: 17259972]

Suarez Y, Fernandez-Hernando C, Yu J, Gerber SA, Harrison KD, Pober JS, Iruela-Arispe ML, Merkenschlager M, Sessa WC. Dicer-dependent endothelial microRNAs are necessary for postnatal angiogenesis. P Natl Acad Sci USA. 2008; 105:14082–14087.

Suarez Y, Sessa WC. MicroRNAs as novel regulators of angiogenesis. Circulation research. 2009; 104:442–454. [PubMed: 19246688]

Suchting S, Freitas C, le Noble F, Benedito R, Breant C, Duarte A, Eichmann A. The Notch ligand Delta-like 4 negatively regulates endothelial tip cell formation and vessel branching. P Natl Acad Sci USA. 2007; 104:3225–3230.

Tammela T, Zarkada G, Wallgard E, Murtomaki A, Suchting S, Wirzenius M, Waltari M, Hellstrom M, Schomber T, Peltonen R, et al. Blocking VEGFR-3 suppresses angiogenic sprouting and vascular network formation. Nature. 2008; 454:656–660. [PubMed: 18594512]

Thurston G, Noguera-Troise I, Yancopoulos GD. The Delta paradox: DLL4 blockade leads to more tumour vessels but less tumour growth. Nature reviews Cancer. 2007; 7:327–331.

Vanhaesebroeck B, Guillermet-Guibert J, Graupera M, Bilanges B. The emerging mechanisms of isoform-specific PI3K signalling. Nature reviews Molecular cell biology. 2010; 11:329–341.

Wang JF, Zhang X, Groopman JE. Activation of vascular endothelial growth factor receptor-3 and its downstream signaling promote cell survival under oxidative stress. The Journal of biological chemistry. 2004; 279:27088–27097. [PubMed: 15102829]

Wang S, Aurora AB, Johnson BA, Qi X, McAnally J, Hill JA, Richardson JA, Bassel-Duby R, Olson EN. The endothelial-specific microRNA miR-126 governs vascular integrity and angiogenesis. Dev Cell. 2008; 15:261–271. [PubMed: 18694565]

Wu L, Fan J, Belasco JG. MicroRNAs direct rapid deadenylation of mRNA. P Natl Acad Sci USA. 2006; 103:4034–4039.

Wu YH, Hu TF, Chen YC, Tsai YN, Tsai YH, Cheng CC, Wang HW. The manipulation of microRNA-gene regulatory networks by KSHV induces endothelial cell motility. Blood. 2011

Yu J, Zhang Y, McIlroy J, Rordorf-Nikolic T, Orr GA, Backer JM. Regulation of the p85/p110 phosphatidylinositol 3′-kinase: stabilization and inhibition of the p110alpha catalytic subunit by the p85 regulatory subunit. Molecular and cellular biology. 1998; 18:1379–1387. [PubMed: 9488453]

Zhu N, Zhang D, Chen S, Liu X, Lin L, Huang X, Guo Z, Liu J, Wang Y, Yuan W, et al. Endothelial enriched microRNAs regulate angiotensin II-induced endothelial inflammation and migration. Atherosclerosis. 2011; 215:286–293. [PubMed: 21310411]

Zygmunt T, Gay CM, Blondelle J, Singh MK, Flaherty KM, Means PC, Herwig L, Krudewig A, Belting HG, Affolter M, et al. Semaphorin-PlexinD1 signaling limits angiogenic potential via the VEGF decoy receptor sFlt1. Developmental cell. 2011; 21:301–314. [PubMed: 21802375]

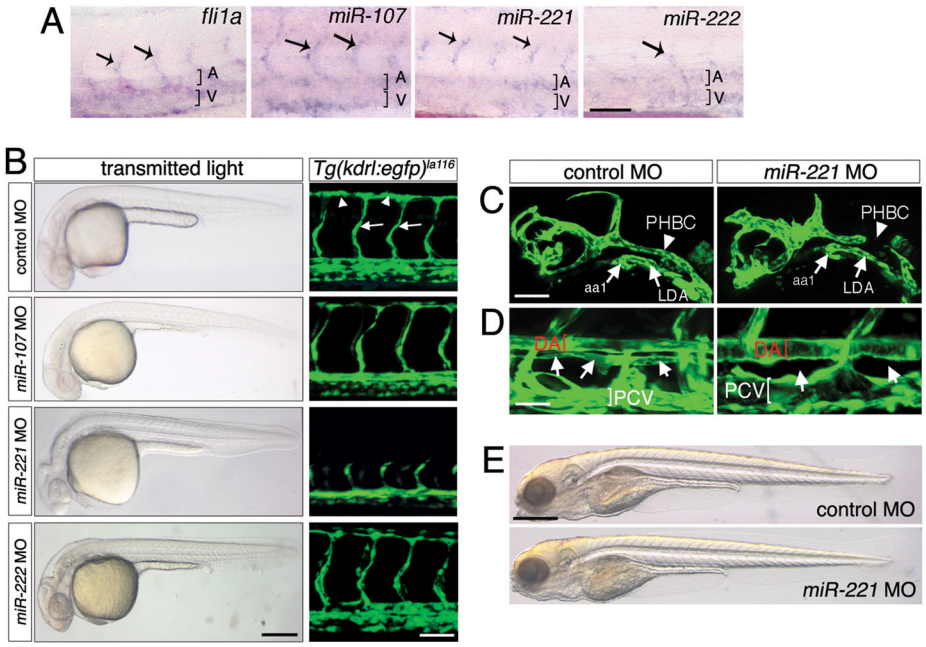

Figure 1. *miR-221* is required for vascular development

(A) Whole mount *in situ* hybridization of embryos at 48 hours post fertilization (hpf). Dorsal aorta and posterior cardinal vein are indicated by a bracket and A or V respectively. Arrows indicate intersegmental blood vessels (ISV). Scale bar = 50 μm. (B) *Left column*, transmitted light images of embryos at 30 hpf injected with indicated MO. Scale bar = 250 μm. *Right column*, confocal micrographs of trunk vessels at 30 hpf in *Tg(kdrl:egfp)*^{la116} embryos injected with indicated MO. ISVs indicated by arrows and dorsal longitudinal anastomtic vessel (DLAV) by arrowheads. Scale bar = 50 μm. (C) *Tg(kdrl:egfp)*^{la116} embryos at 27 hpf injected with 10 ng control or *miR-221* MO. aa1 – aortic arch 1, PHBC – primordial hindbrain channel, LDA – lateral dorsal aorta. Scale bar = 50 μm. (D) *Tg(fli1a:egfp)*^{y1} embryos at 5 days post fertilization (dpf) injected as in (C). DA – dorsal aorta, PCV – posterior cardinal vein; position of thoracic duct is indicated by arrows. Scale bar = 25 μm. (E) Transmitted light images of larvae at 5 dpf injected as in (C). Scale bar = 500 μm. All panels are lateral views, dorsal is up, anterior to the left.

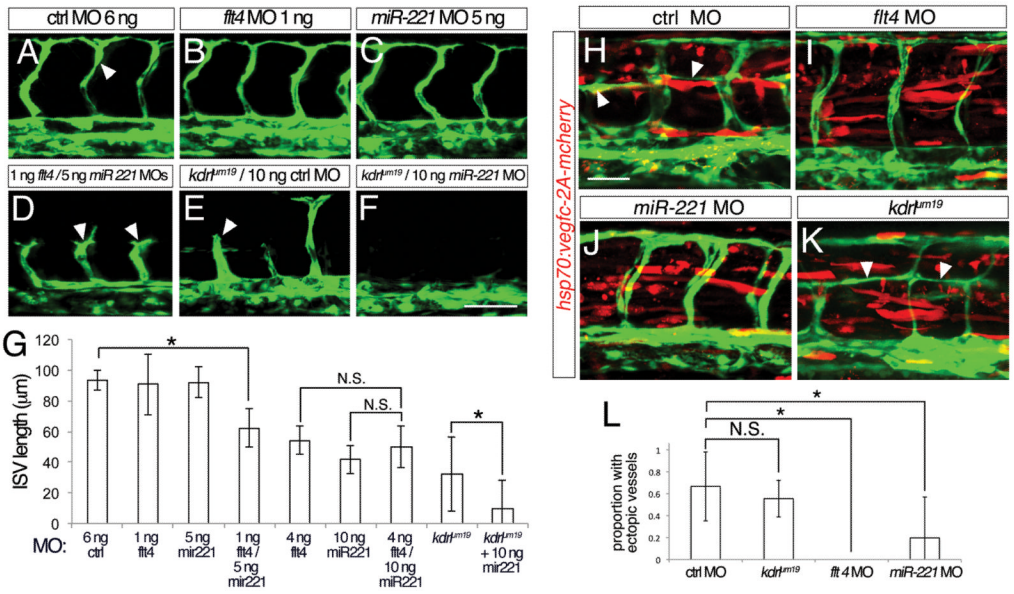

Figure 2. *miR-221* is required for Vegfc/Flt4 signaling

(A–F) Confocal micrographs *Tg(fli1a:egfp)*^{y1} embryos at 27 hpf; arrowheads denote ISVs; lateral views, dorsal is up, anterior to the left. (A) Embryo injected with 6 ng control MO. (B) Embryo injected with 1 ng *flt4* and 5 ng control MO. (C) Embryo injected with 1 ng control and 5 ng *miR-221* MO. (D) Embryo injected with 1 ng *flt4* MO and 5 ng *miR-221* MO. (E) *kdrl*^{um19} mutant embryo injected with 10 ng control MO. (F) *kdrl*^{um19} mutant embryo injected with 10 ng of *miR-221* MO. (G) Quantification of ISV length in wild type or *kdrl*^{um19} mutant embryos injected with indicated MO(s). Measurements were made of 4 adjacent ISVs per embryo in at least 18 embryos from 3 separate injections; * $p<0.001$; N. S. – not statistically different. (H–K), *Tg(fli1a:egfp)*^{y1} embryos injected with *hsp70:vegfc-2A-mcherry* transposable element and heat shocked at 15 ss. Red indicates Vegfc-2A-mcherry expression. Arrowheads indicate ectopic formation of vessels. Embryos at 33 hpf co-injected with (H) 10 ng control MO, (I) 2 ng *flt4* MO, (J) 10 ng *miR-221* MO, or (K) mutant for *kdrl*^{um19}. (L) Proportion of hemisegments with ectopic vessel sprouts in embryos injected with 25 pg Tol2-hsp70:vegfc-2A-mcherry and 25 pg Tol2 transposase. Embryos were co-injected with indicated MO, or were mutant for the *kdrl*^{um19} allele as determined by genotyping following phenotypic analysis. * $p<0.02$; N.S. – not significant. Scale bars are (A–F) 50 µm and (H–K) 25 µm.

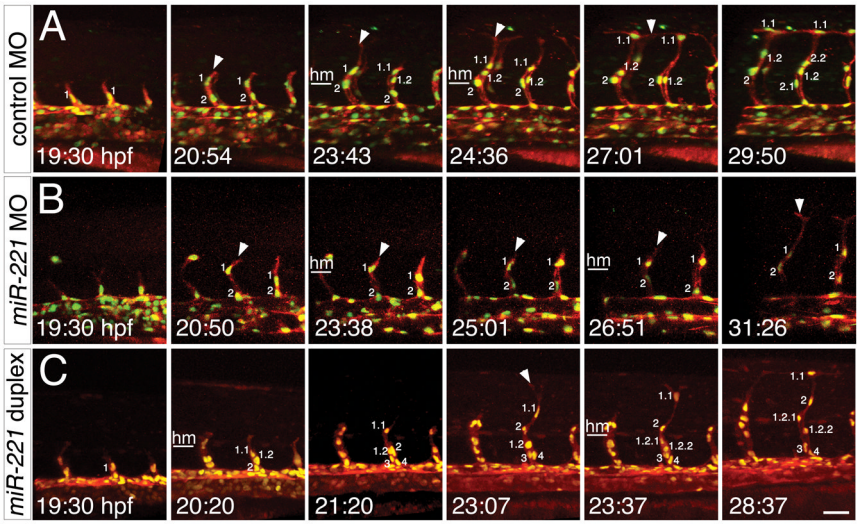

Figure 3.

miR-221 regulates migration and proliferation of tip cells. (A–C) Still images from time-lapse analysis of (A,B) *Tg(fli1a:negfp)*^{y7}*;(kdrl:ras-cherry)*^{s916} or *Tg(fli1a:negfp)*^{y7}*; (kdrl:tagrfap-caax)*^{is7} embryos. Time (hpf) is noted in the bottom left hand corner. Nuclei are numbered; successive numbers indicate new cells that migrated from the dorsal aorta, decimals indicate daughter cells arising from cell division. Lateral views, dorsal is up, anterior to the left. Horizontal white line denotes horizontal myoseptum (hm). (A) Embryo injected with 10 ng control MO. (B) Embryo injected with 10 ng *miR-221* MO. (C) Embryo injected with 500 μM *miR-221* duplex. Scale bar is 25 μm.

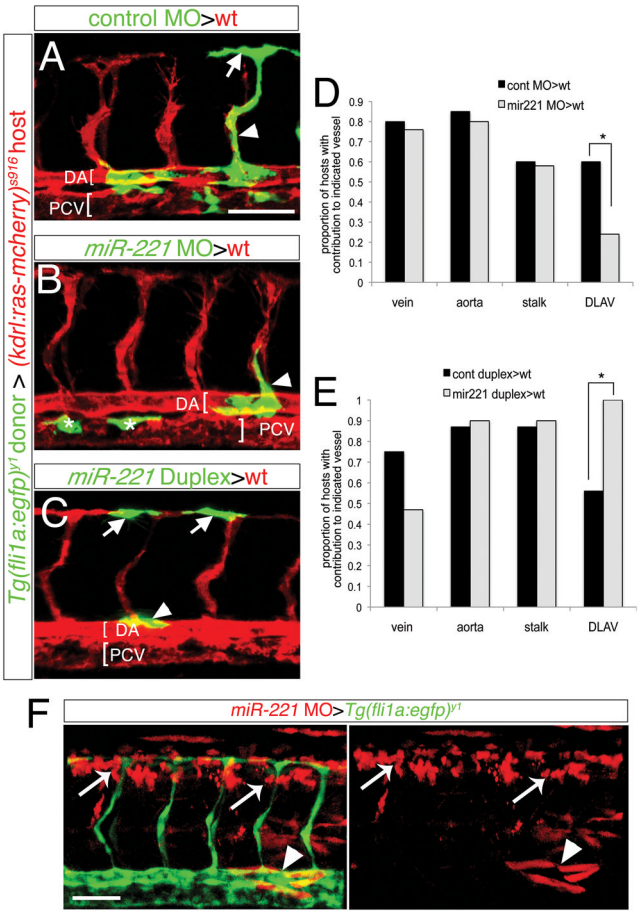

Figure 4. *miR-221* acts endothelial cell autonomously to drive tip cell potential

(A–C, F), Confocal micrographs of mosaic embryos at 27 hpf following cell transplantation. (A–C) Donor *Tg(fli1a:egfp)*^{y1} cells are green, host *Tg(kdrl:ras-mcherry)*^{s916} vessels are red; DA – dorsal aorta, PCV – posterior cardinal vein, both indicated by brackets. (A) Donor control cells in DLAV (arrow) and ISV stalk (arrowhead). (B) Donor *miR-221* deficient cells in the ISV stalk (arrowhead). Asterisks indicate donor cells in the PCV. (C) Donor cells over-expressing *miR-221* in DLAV (arrows) and dorsal aorta (arrowhead). (D, E) Proportion of host embryos with donor contribution to indicated blood vessel type. (D) * p=0.04. (E) * p=0.001. (F) *Tg(fli1a:egfp)*^{y1} host embryo with *miR-221* deficient donor cells labeled with rhodamine in non-endothelial cell types surrounding the ISVs, including neural tube (white arrows) and somites (white arrowheads). Scale bars are 50 μm.

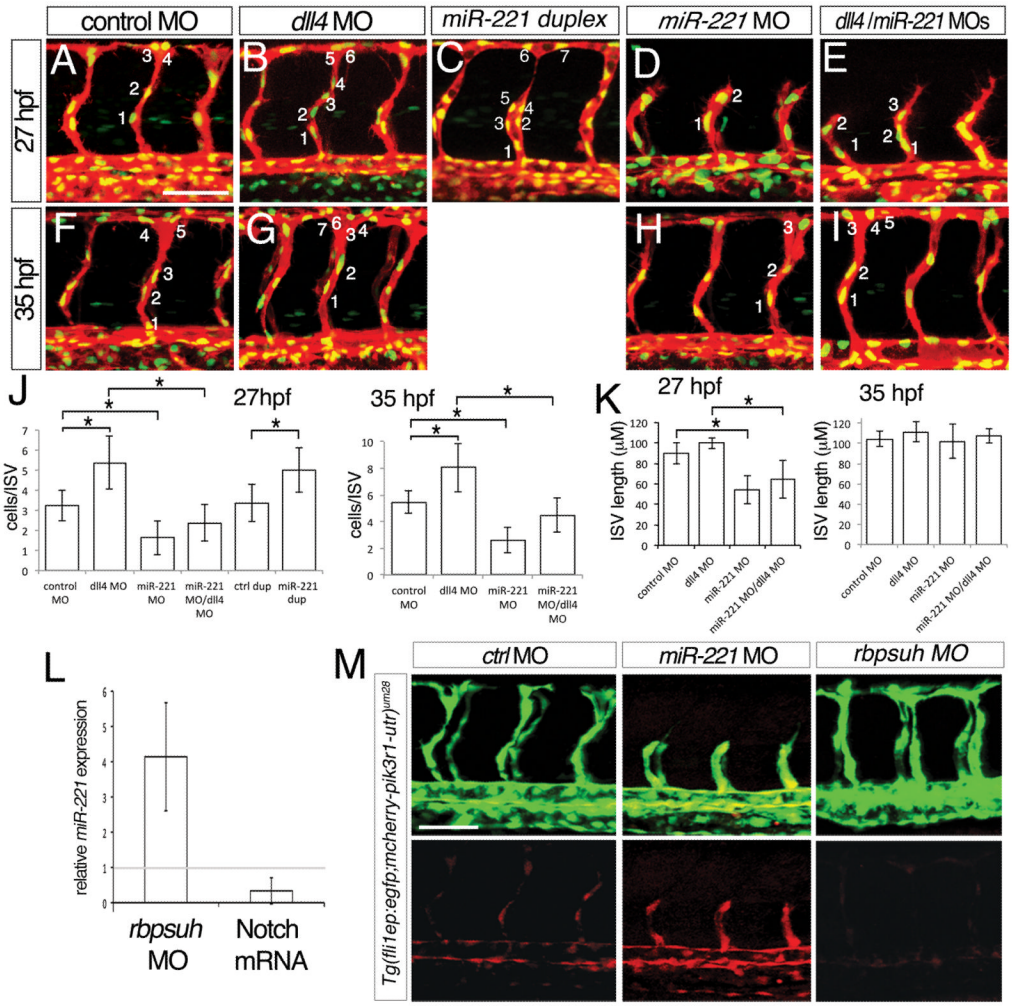

Figure 5. *miR-221* is required for the Notch-deficient "hyper" h-angiogenesis phenotype

(A–I), Confocal micrographs of *Tg(fli1a:negfp)*^{y7}*;(kdrl:ras-cherry)*^{s916} embryos, lateral views, dorsal is up, anterior to the left. Numbers indicate nuclei in representative intersegmental blood vessels (ISV). (A–E) Embryos at 27 hours post fertilization (hpf). (F–I) Embryos at 35 hpf. (A, F) Embryos injected with 25 ng of control MO. (B, G) Embryos injected with 15 ng of *dll4* MO. (C) Embryo injected with 500 μM *miR-221* duplex. (D, H) Embryo injected with 10 ng of miR-221 MO. (E, I) Embryos co-injected with 15 ng of *dll4* MO and 10 ng of *miR-221* MO. (J) Quantification of endothelial number and (K) ISV length in *Tg(fli1:ngfp)*^{y7}*;(kdrl:ras-cherry)*^{s916} embryos injected with indicated MO(s);* p-value < 0.0001. Measurements were determined for 4 adjacent ISVs per embryo in at least 8 embryos from 3 separate injections. (L) Fold change of mature *miR-221* levels assessed by qRT-PCR in embryos injected with 2.5 ng *rbpsuh* MO or with mRNA encoding an activated form of Notch compared to control embryos. (M) Confocal micrographs of *Tg(fli1ep;mcherry-pik3r1-utr)*^{um28} embryos injected with 10 ng control MO, 10 ng *miR-221* MO, or 2.5 ng Rbpsuh MO. Lateral views, dorsal is up, anterior to the left. Scale bars are 50 μm.

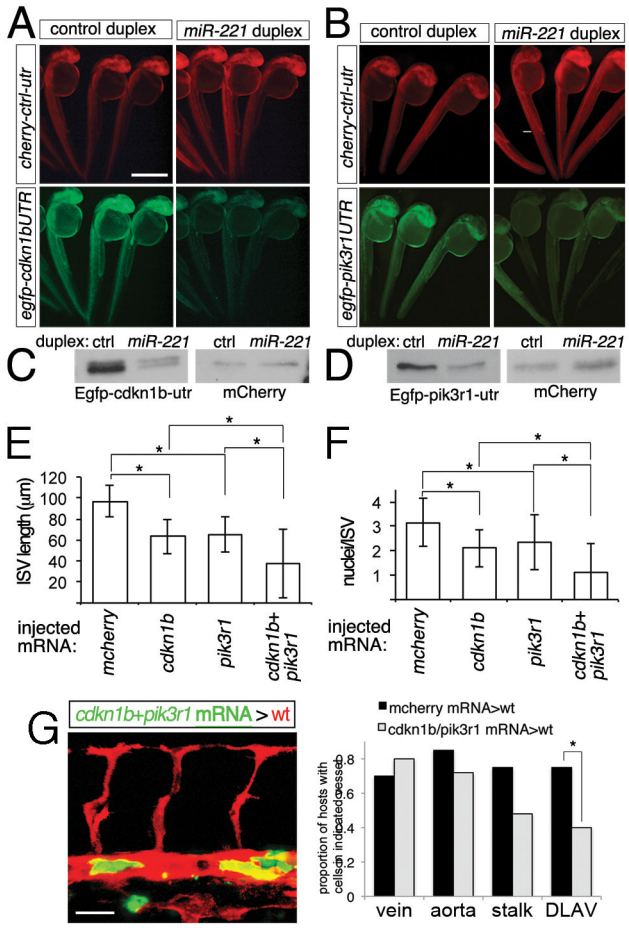

Figure 6. *cdkn1b* and *pik3r1* are targets of *miR-221*

(A, B) Fluorescent images and of embryos co-injected with 150 pg each of *mcherry* mRNA fused to control 3′ untranslated region (utr) and *egfp* mRNA fused to (A) *cdkn1b* 3′UTR or (B) *pik3r1* 3′UTR with 100μM indicated duplex RNA. Lateral views, dorsal is up, anterior to the left. Scale bar is 500 μm. (C, D) Western analysis of embryos in (A, B). (E) ISV length and (F) cell number in *Tg(fli1:egfp)*^{y1} and *Tg(fli1:negfp)*^{y7} embryos, respectively, at 27 hpf injected with 500 pg of indicated mRNAs. For co-injections, 200 pg of *cherry2A-cdkn1b* and 300 pg *cherry2A-pik3r1* mRNA were used. *p-value < 0.002. (G) *Left*, host *Tg(kdrl:ras-mcherry)*^{s916} embryo at 27 hpf following transplantation of cells from a *Tg(fli1a:egfp)*^{y1} embryo injected with 200 pg *cdkn1b* and 300 pg *pik3r1* mRNA *Right*, proportion of embryos displaying donor cells in indicated vessel type. Control donor cells were from embryos injected with 500 pg *mcherry* mRNA. * p=0.03. Scale bar is 25 μm.

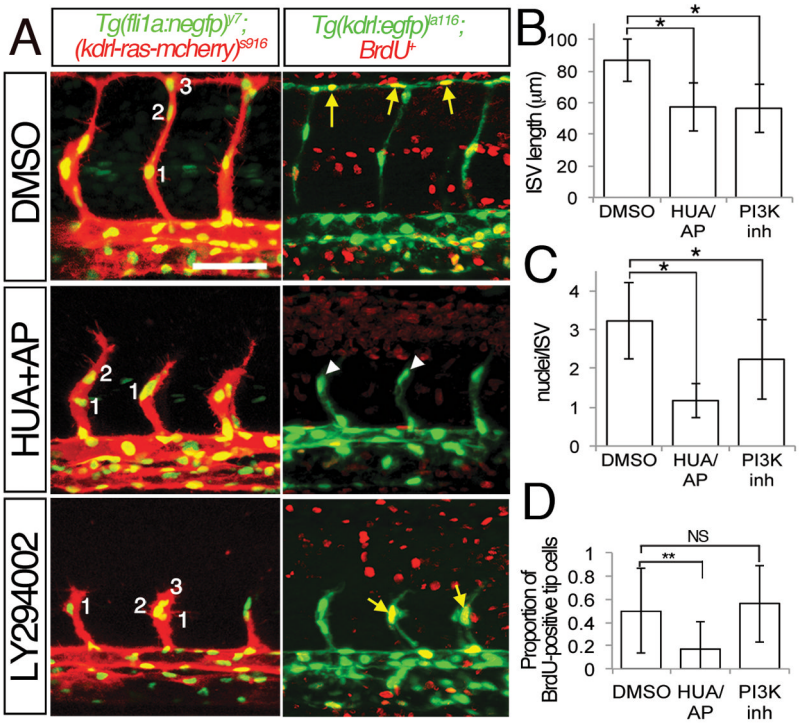

Figure 7. Proliferation and PI3K are required for ISV growth

(A) Embryos at 27 hpf treated with 4% DMSO, 150 μM 5-hydroxyurea and 20 mM aphidocolin (HUA/AP), or 25 μM LY294002 (PI3K inh) beginning at 20 hpf. *Left panels*, confocal micrographs of *Tg(fli1:negfp)*^{y7}*;(kdrl:ras-cherry)*^{s916} embryos; *right panels*, two-photon micrographs of *Tg(kdrl:egfp)*^{la116} embryos pulsed with BrdU at 20 hpf. Lateral views, dorsal is up, anterior to the left, yellow arrows denote BrdU-positive endothelial nuclei; BrdU-negative endothelial nuclei indicated by white arrowheads. Scale bar is 50 μm. (B, C) Quantification of (B) ISV length in microns and (C) number of nuclei per ISV in *Tg(fli1:negfp)*^{y7}*;(kdrl:ras-cherry)*^{s916} embryos at 27 hpf treated as in (A). *p<0.0001 (D) Quantification of BrdU-positive DLAV or ISV tip cells in *Tg(kdrl:egfp)*^{la116} embryos at 27 hpf treated as in (A). ** $p < 0.02$. NS – not significant.

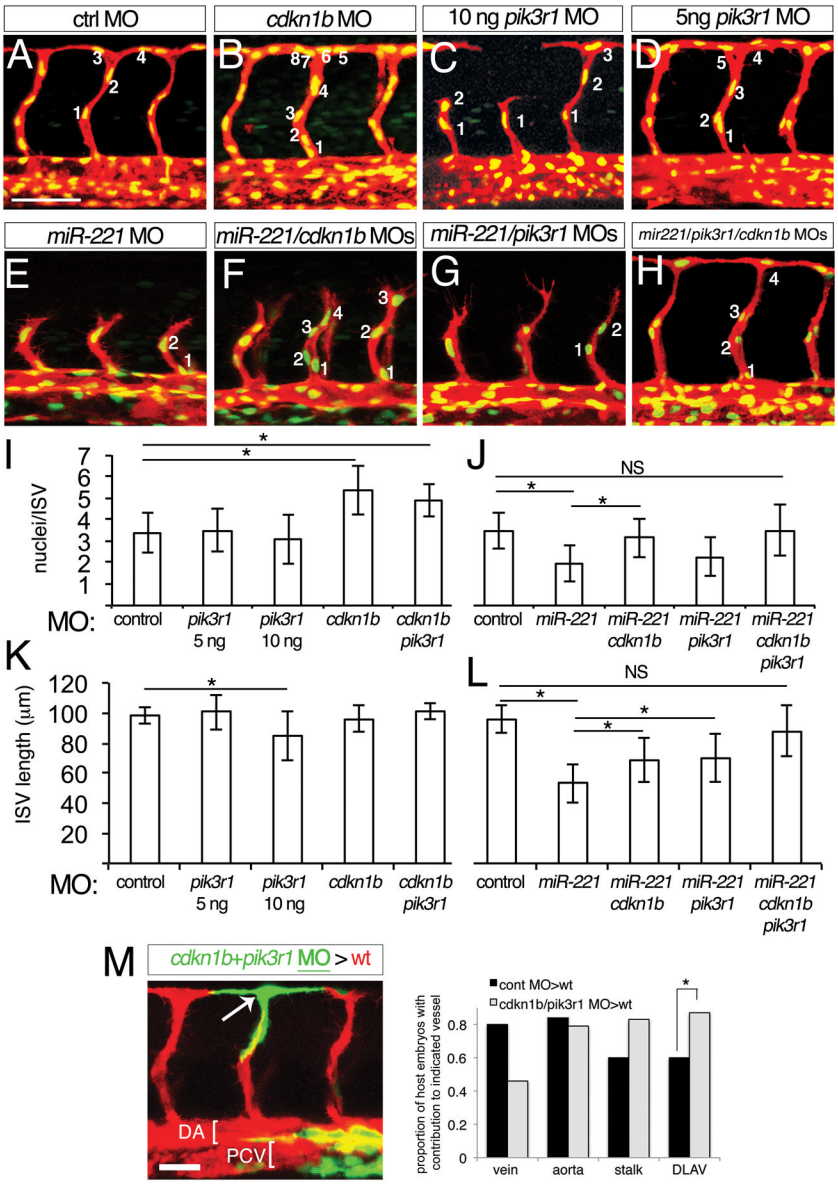

Figure 8. *pik3r1* and *cdkn1b* are functional downstream targets of miR-221

(A–H) *Tg(fli1a:negfp)*^{y7}*;(kdrl:ras-cherry)*^{s916} embryos at 27 hpf. Numbers denote cell nuclei of representative ISV. All embryos were co-injected with 1 ng of *p53* MO. Scale bars is 50 μm. Embryo injected with (A) 15 ng control MO (B) 5 ng *cdkn1b* MO, (C) 10 ng *pik3r1* MO, (D) 5 *pik3r1* MO, (E) 10 ng *miR-221* MO, (F) 10 ng *miR-221* and 5 ng *cdkn1b* MOs, (G) 10 ng *miR-221* and 5 ng *pik3r1* MOs, (H) 10 ng miR-221, 3 ng *cdkn1b* and 3 ng *pik3r1* MOs. (I, J) Quantification of cells per ISV and (K, L) ISV length in embryos at 27 hpf injected with MOs as above, except control MO, which was injected at (I, K) 10 ng and (J, L) 15 ng doses. *p<0.001; N.S. – not significant. Measurements were obtained from 4 adjacent ISVs in at least 10 embryos from three separate experiments. (M) *Left*, host *Tg(kdrl:ras-mcherry)*^{s916} embryo at 27 hpf following transplantation of cells from a *Tg(fli1a:egfp)*^{y1} embryo injected with 3 ng *cdkn1b* MO and 5 ng *pik3r1* MO. *Right*, proportion of embryos displaying donor cells in indicated vessel type. Data from control donor cells is the same as in Fig. 4D. *p=0.07. Scale bar is 25 μm.